

Type IV Pilus Structure by Cryo-Electron Microscopy and Crystallography: Implications for Pilus Assembly and Functions

Lisa Craig,¹ Niels Volkmann,² Andrew S. Arvai,³ Michael E. Pique,³ Mark Yeager,⁴ Edward H. Egelman,^{6,*} and John A. Tainer^{5,*}

¹Department of Molecular Biology and Biochemistry
Simon Fraser University
Burnaby, British Columbia V5A 1S6
Canada

²The Burnham Institute

³Department of Molecular Biology

⁴Department of Cell Biology

⁵Department of Molecular Biology and
The Skaggs Institute for Chemical Biology
The Scripps Research Institute
La Jolla, California 92037

⁶Department of Biochemistry and Molecular Genetics
University of Virginia Health Sciences Center
Charlottesville, Virginia 22908

Summary

Type IV pili (T4P) are long, thin, flexible filaments on bacteria that undergo assembly-disassembly from inner membrane pilin subunits and exhibit astonishing multifunctionality. *Neisseria gonorrhoeae* (gonococcal or GC) T4P are prototypic virulence factors and immune targets for increasingly antibiotic-resistant human pathogens, yet detailed structures are unavailable for any T4P. Here, we determined a detailed experimental GC-T4P structure by quantitative fitting of a 2.3 Å full-length pilin crystal structure into a 12.5 Å resolution native GC-T4P reconstruction solved by cryo-electron microscopy (cryo-EM) and iterative helical real space reconstruction. Spiraling three-helix bundles form the filament core, anchor the globular heads, and provide strength and flexibility. Protruding hyper-variable loops and posttranslational modifications in the globular head shield conserved functional residues in pronounced grooves, creating a surprisingly corrugated pilus surface. These results clarify T4P multifunctionality and assembly-disassembly while suggesting unified assembly mechanisms for T4P, archaeal flagella, and type II secretion system filaments.

Introduction

T4P are multifunctional membrane-anchored filaments essential for the virulence of many Gram-negative bacterial pathogens, including *Neisseria gonorrhoeae* and *N. meningitidis* (Merz and So, 2000), enteric pathogens such as *Vibrio cholerae* (Taylor et al., 1987), *Escherichia coli* (Giron et al., 1991), and *Salmonella typhi* (Zhang et al., 2000), and the potential bioterrorism agent *Francisella tularensis* (Gil et al., 2004). T4P serve remarkably diverse functions, including bacterial motility, adhesion, microcolony, and biofilm formation, natural transformation, and immune escape (reviewed in Craig et al.

[2004]). Biological interest in T4P is enhanced by their genetic and structural similarities to the archaeal flagellar and type II secretion systems (Peabody et al., 2003) and by their application as vaccines and nanotechnology components for DNA binding (Audette et al., 2004; Boslego et al., 1991; Taylor et al., 2004).

T4P are extremely thin (~60–80 Å), long (>1 μm) filaments, which can withstand >100 pN of stress force (Maier et al., 2002) to combat the strong shear forces bacteria face when attached to host cell surfaces. These versatile filaments are comprised of thousands of copies of a single subunit, pilin. Three-dimensional structural analyses of T4P have proved extremely challenging due to the fiber-forming tendencies and membrane associations of pilin subunits and the thinness and apparent featurelessness of the pilus filaments (Craig et al., 2004). Only two structures of full-length pilin proteins have been solved to date: platinum-modified *N. gonorrhoeae* PilE (gonococcal or GC pilin) (Parge et al., 1995) and *Pseudomonas aeruginosa* PilA (PAK pilin) (Craig et al., 2003). These structures, together with structures of truncated pilins lacking the protruding hydrophobic N-terminal α helix (Audette et al., 2004; Craig et al., 2003; Keizer et al., 2001; Xu et al., 2004), reveal an α+β structural scaffold with distinct topologies for the fold of the globular head. Low-resolution EM and X-ray fiber diffraction analyses have suggested useful filament models consistent with the smooth appearance of T4P in electron micrographs. However, a detailed prototypic structure would help to address unanswered questions regarding T4P assembly and diverse functions and also to integrate genetic, biochemical, and functional results on T4P.

Among the well-characterized and medically important T4P of human pathogens, the *N. gonorrhoeae* GC-T4P provide a suitable prototype for systematic structure-function characterizations (Merz and So, 2000). *N. gonorrhoeae* causes the sexually transmitted disease gonorrhea. GC-T4P play essential and diverse roles in *N. gonorrhoeae* colonization of the human urogenital tract. T4P undergo dynamic assembly and disassembly from a reservoir of pilin subunits in the inner membrane for twitching motility (Morand et al., 2004), which allows movement on epithelial surfaces at rates of ~1 μm per second (Merz et al., 2000). GC-T4P mediate attachment of *Neisseriae* to host epithelial cells and to each other to form microcolonies for protection against the host immune response (Rudel et al., 1995). GC-T4P are also required for natural transformation (Aas et al., 2002), which maintains genetic diversity, and are implicated in Ca²⁺ signaling (Ayala et al., 2005) and modulating the host immune response (Plant and Jonsson, 2006).

A major puzzle for GC-T4P assembly involves the bacteria's ability to continually modify its pilin sequence to avoid a protective immune response (Criss et al., 2005). Immune evasion by GC-T4P can therefore result in persistent, repeated gonorrheal infections and lead to infertility, arthritis, endocarditis, and meningitis. This extreme sequence variation arises from recombination between the expressed pilin gene *pilE* and several silent

*Correspondence: egelman@virginia.edu (E.H.E.); jat@scripps.edu (J.A.T.)

pilS genes (Haas and Meyer, 1986; Segal et al., 1986; Swanson et al., 1986) and may be a function of ploidy in the *N. gonorrhoeae* genome (Tobiason and Seifert, 2006). Thus, a human vaccine trial employing a single GC-T4P variant produced an anti-pilus response but no protection against subsequent challenge (Boslego et al., 1991). A detailed knowledge of GC-T4P structural chemistry would provide insights into the mechanistic basis for a filament assembly that allows sequence variation and diverse functions and may suggest new therapeutic strategies that use T4P as effective protein epitope carriers, immunogens, and targets for inhibitors that block binding to host cells and biofilm surfaces (Giltner et al., 2006; Hsieh et al., 2005).

Here, we report a high-resolution crystal structure of an endogenously expressed and posttranslationally modified full-length pilin subunit and a 3D cryo-EM reconstruction of the pilus filament, both derived from the same *N. gonorrhoeae* strain. The unique computational fit for the pilin subunit into the cryo-EM density map generated a high-resolution T4P filament structure. The combined results help clarify the T4P assembly mechanism and resolve the paradox between the conserved architecture and multifunctionality of T4P in pathogenicity.

Results and Discussion

Native GC Pilin Crystal Structure, Posttranslational Modifications, and Altered Amino Acid Sequence

To accurately define T4P structure and assembly, we determined both a high-resolution crystal structure of the pilin subunit and a cryo-EM reconstruction of the pilus filament from the same *N. gonorrhoeae* C30 strain. Native GC-T4P (Figure 1) were purified from *N. gonorrhoeae* and flash-cooled for cryo-EM analysis or dissociated by detergent into pilin subunits for crystallization and high-resolution structure determination (see the Supplemental Data available with this article online). We determined a 2.3 Å resolution crystal structure of the full-length endogenously expressed GC pilin protein (Table 1 and Figure 2). The high-quality electron density map revealed posttranslational modifications at Ser63 (Figures 2A and 2B) and Ser68 (Figures 2A and 2C) and sequence differences for this *N. gonorrhoeae* strain (Figure 2D).

GC pilin is an elongated ladle-shaped molecule (Figure 2A). The sequence-conserved N-terminal 53 residues comprise an 85 Å long S-shaped α -helical handle, α 1. The N-terminal half of α 1 (α 1-N, residues 1–29) protrudes, whereas the C-terminal half (α 1-C, residues 30–53) is wrapped by an antiparallel four-stranded β sheet to form the globular head domain, which is a hallmark of the type IV pilins (Craig et al., 2003). The $\alpha\beta$ loop (residues 53–71) joining the N-terminal α helix and the β sheet contains a short α helix and two posttranslational modifications that protrude from the globular domain to form a ridge on the subunit surface (Figures 2A–2C). On the opposite side of the β sheet, the disulfide or D region, delineated by the Cys121-to-Cys151 disulfide bond, forms a β hairpin containing the hypervariable loop (residues 128–141), which protrudes as a second ridge on the globular domain.

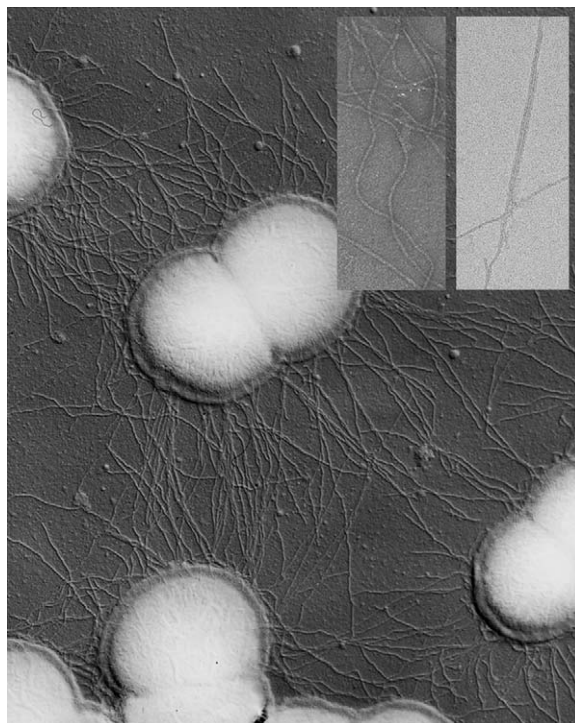


Figure 1. Type IV Pili (T4P) on *N. gonorrhoeae*. Scanning EM (courtesy of Charles Brinton) shows >1 μ m long, thin (~60 Å diameter) T4P filaments distributed peritrichously on *N. gonorrhoeae* diplococci. Transmission EM insets of negatively stained GC-TCP show pilus flexibility and bundle-forming tendencies.

The clear electron density map for the O-linked disaccharide at $\alpha\beta$ loop Ser63 defines a new sugar for GC pilin: α -D-galactopyranosyl-(1 \rightarrow 3)-2,4-diacetamido-2,4-dideoxy- β -D-glucopyranoside or Gal-DADDGlc (Figure 2B). This sugar moiety has a second acetamido

Table 1. GC Pilin Crystallographic Diffraction Data and Refinement Statistics

Beamline (SSRL)	7-1
Space group	C222
Cell a, b, c (Å)	119.754, 124.941, 26.848
Cell $\alpha\beta\gamma$	90.00, 90.00, 90.00
Resolution (Å)	2.3
Wavelength (Å)	1.08
Completeness (%) ^a	93.2/71.8
Observed reflections	27,478
Unique reflections	8868
R _{sym} (%) ^{a,b}	5.8/23.6
I/ σ ^a	21.5/3.2
Mosaicity	1.00
Refinement Statistics	
Resolution (Å)	40–2.30
Molecules/AU	1
R _{cryst} (%) ^c	25.6
R _{free} (%) ^d	28.1
Average B factor (Å ²)	43.4

^a Overall/last shell.

^b $R_{sym} = \sum (|I_{hkl}| - \langle I \rangle) / \sum I_{hkl}$, where I_{hkl} is the integrated intensity of a given reflection.

^c $R_{cryst} = \sum |hkl| |F_{obs}(hkl)| - |F_{calc}(hkl)| / \sum |hkl| |F_{obs}(hkl)|$.

^d R_{free} calculated for 5% of all reflections that were excluded from refinement.

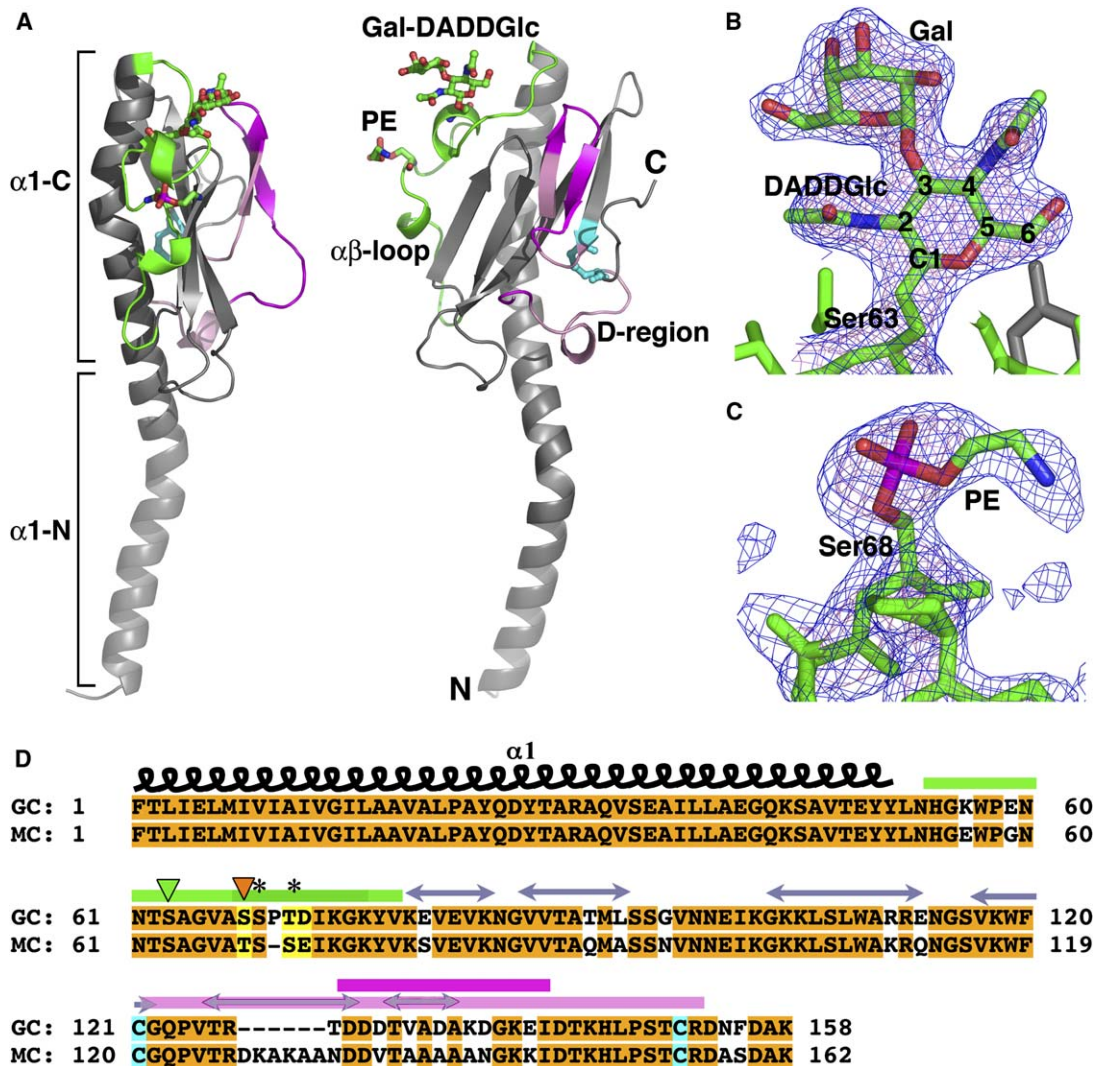


Figure 2. Full-Length GC Pilin Crystal Structure and Sequence Alignment with MC Pilin

(A) Side (left) and front (right) pilin subunit views show regions conserved among the type IV pilins (gray), including the extended N-terminal α helix $\alpha 1$ (comprised of $\alpha 1$ -N and $\alpha 1$ -C), the β sheet and the disulfide (cyan), plus the structurally variable D region (pink) with the hypervariable loop on the β hairpin (magenta) and the $\alpha\beta$ loop (green) with the disaccharide Gal-DADDGlc and phosphoethanolamine (PE).

(B and C) Gal-DADDGlc (B) at Ser63 and phosphoethanolamine (C) at Ser68 shown with 2F_o - F_c electron density map (blue, 1 σ ; pink, 2 σ).

(D) Sequence alignment of GC (*N. gonorrhoeae* strain C30) and MC (*N. meningitidis* MC58, NCBI Accession AE002098) pilin with identical (orange) and conserved (yellow) residues highlighted. Structural features on GC pilin are shown as follows: disulfide cysteines, cyan; Ser63 disaccharide, green arrowhead; Ser68 phosphoethanolamine, orange arrowhead; Ser69 and Thr71 sequence differences from the previous structure, asterisks; β strands, arrows; $\alpha\beta$ loop, green bar; and D region with hypervariable loop (pink and magenta bars, respectively).

group at C4 of the proximal glucose in place of the hydroxyl group seen in the earlier GC pilin crystal structure (Parge et al., 1995). DADDGlc thus resembles 2,4-diacetamido-2,4,6-trideoxyhexose, or DATDH, which is a constituent of a disaccharide on GC pilin from *N. gonorrhoeae* strain N400 (Hegge et al., 2004) and of a trisaccharide on the closely related MC pilin from *N. meningitidis* (Figure 1D) (Stimson et al., 1995). However, DATDH lacks the C6 hydroxyl group that was defined in our electron density map (Figure 2B).

The ability of pathogenic *Neisseriae* to glycosylate pilin may affect pilus interactions with nearby pili, host receptors, and antibodies. Mutation of Ser63 to Ala in MC pilin eliminates glycosylation and increases pilus bundling, suggesting the sugar is exposed and contributes to surface chemistry (Marceau et al., 1998; Stimson

et al., 1995). In *N. meningitidis*, but not *N. gonorrhoeae*, Ser63 glycosylation is essential for production of S pilin, a naturally expressed soluble pilin variant (Marceau and Nassif, 1999). On GC-T4P, the exposed Ser63 carbohydrate may prevent antibody recognition by mimicking “self” carbohydrate antigens. Carbohydrate phase variation, as seen for MC pilin (Power et al., 2003), would aid immune evasion.

The extended electron density at $\alpha\beta$ loop Ser68 is consistent with phosphoethanolamine (Figure 2C). Rerefinement of the prior 2.6 Å pilin electron density map with phosphoethanolamine instead of the published phosphate modification (Forest et al., 1999) produced negative density, confirming the earlier identification and suggesting differential posttranslational modification of Ser68. Mass spectrometry analysis similarly showed

differential modification of *N. gonorrhoeae* strain N400 GC pili, such that a peptide spanning Ser68 can possess phosphoethanolamine, phosphocholine, or no modification (Hegge et al., 2004), and a phosphocholine epitope identified on both *N. gonorrhoeae* and *N. meningitidis* was found to undergo phase variation (Weiser et al., 1998). Negatively charged phosphates and positively charged amino and choline moieties would alter the GC-T4P surface chemistry, which could affect pilus interactions and host immune recognition.

The electron density also indicated $\alpha\beta$ loop sequence changes compared to the previous GC pilin structure, with serine replacing Pro69 and threonine replacing Ser71. These changes, as confirmed by sequencing the *pilE* gene (Figure 2D), likely represent recombination-induced antigenic variation and suggest that the GC subunit readily accommodates variation at these positions.

Three-Dimensional Cryo-EM Reconstruction of the GC-T4P Filament

To understand how GC pilin subunits assemble into thin, strong, multifunctional filaments, we applied the iterative helical real space reconstruction (IHRSR) algorithm (Egelman, 2000) to cryo-EM images of frozen-hydrated GC-T4P filaments (Figure 3A). We determined the approximate pilus symmetry by boxing filaments on digitized cryo-EM images and calculating an averaged power spectrum, revealing five layer lines (Figure 3B). From the axial position of the layer lines and the intensity peak positions along these layer lines, the helical symmetry was defined as ~ 3.6 subunits per turn of a 37 Å pitch 1-start helix. We used this symmetry estimate to generate initial reference volumes, to which the individual filament segments were aligned by the IHRSR method (see Supplemental Data). Reference volumes with substantially different symmetries either failed to converge to a reasonable reconstruction or generated unphysical solutions, thereby validating the symmetry estimate. Two GC-T4P cryo-EM reconstructions were generated, which differed in the number of filament segments used, the defocus range, and the approach to contrast transfer function (CTF) correction (Supplemental Data). Comparison of these two reconstructions by the Fourier shell correlation method (Harauz and van Heel, 1986) (FSC, threshold 0.50) provided a resolution estimate of 12.5 Å. This estimate is conservative because it compares two independent data sets, in contrast to the standard FSC method that typically compares two halves of a single data set processed by identical methods and aligned to the same reference (Yang et al., 2003). To minimize artifacts from amplitude distortion caused by the CTF and other experimental factors, we corrected the cryo-EM density maps by scaling the amplitudes to the spherically averaged molecular transform of the resulting filament model (Figures 3C–3H, see below).

The resulting GC-T4P 3D reconstruction is marked by high ridges and deep grooves that wind around the filament axis (Figure 3C). Color coding by radial distance from the filament axis (Figure 3D) reveals the remarkably corrugated nature of the GC-T4P surface, which contrasts to the smooth filament modeled from low-resolution EM images (Parge et al., 1995). The filament interior is tightly packed but has an unanticipated narrow cen-

tral channel (Figure 3E). The deep grooves in the pilus surface (blue and green, Figure 3D) run alongside a repeating donut-shaped mass (red and yellow) with a central depression (green). When filtered to match the resolution of the cryo-EM reconstruction, the crystal structure of the GC pilin globular head domain aligns well with this repeating mass (Figures 3F and 3G), placing the N-terminal α helix ($\alpha 1$) within the filament core almost parallel to the filament axis. The protruding $\alpha\beta$ loop and D regions of the pilin subunit align with the protruding ridges of the donut-like surface feature of the reconstruction, and the β sheets line the bottom of the central depressions (Figures 3G and 3H). The pilin subunits fit into only one of the two reconstruction enantiomorphs, where they are related by a 10.5 Å rise and a 100.8° azimuthal rotation along a right-handed 1-start helix (see Figure 4A).

GC-T4P Filament Structure at High Resolution

The GC pilin crystal structure was quantitatively and objectively fit into the GC-T4P reconstruction based on real-space correlations between the electron and EM density maps using the CoAn suite of programs (Volkman and Hanein, 2003) (see Supplemental Data). We tested both the 2.3 and the 2.6 Å resolution GC pilin crystal structures in the docking experiments as full-length and truncated models lacking the protruding N-terminal 28 residues. Densities for these four pilin models were fit to both enantiomorphs of the two independent EM reconstructions in 16 separate experiments, each generating a set of solutions. Filament models, built by applying the symmetry operators defined by the reconstruction to the docked pilin solutions, placed the N-terminal $\alpha 1$ α helices inside the central core of the observed EM density with no significant steric clashes between neighboring subunits. Minor clashes were removed with a regularization algorithm that enforces stereochemical constraints. Notably, no information about the neighboring subunits (nor the missing $\alpha 1$ residues in the truncated pilin models) was introduced at any stage. Therefore, the excellent packing of the 85 Å long $\alpha 1$ α helices within the ~ 60 Å diameter EM density independently validated the cryo-EM reconstruction and docking procedures.

To generate a consensus model of the filament, we selected the top fit in the solution sets that also exhibited the fewest unfavorable main-chain contacts with its neighbors. The extreme N terminus (residues 1–4), which has different conformations for the two GC pilin crystal structures, was remodeled to eliminate steric clashes. The resulting computationally derived fit of the pilin subunit within the pilus filament resembles that obtained manually, suggesting that the reconstruction determined a single unique solution.

Previous GC-T4P models predicted tightly packed globular heads with a continuous β sheet wrapping the filament (Parge et al., 1995). Yet, in this high-resolution pilus structure, pilin heads are separated by deep grooves and subunits are held together predominantly by extensive packing of the hydrophobic N-terminal α helices in the filament core (Figures 4A–4D). The reconstruction also identifies polar interactions among the globular head domains at the base of the grooves: the $\alpha\beta$ loop of one subunit and the D region of the next

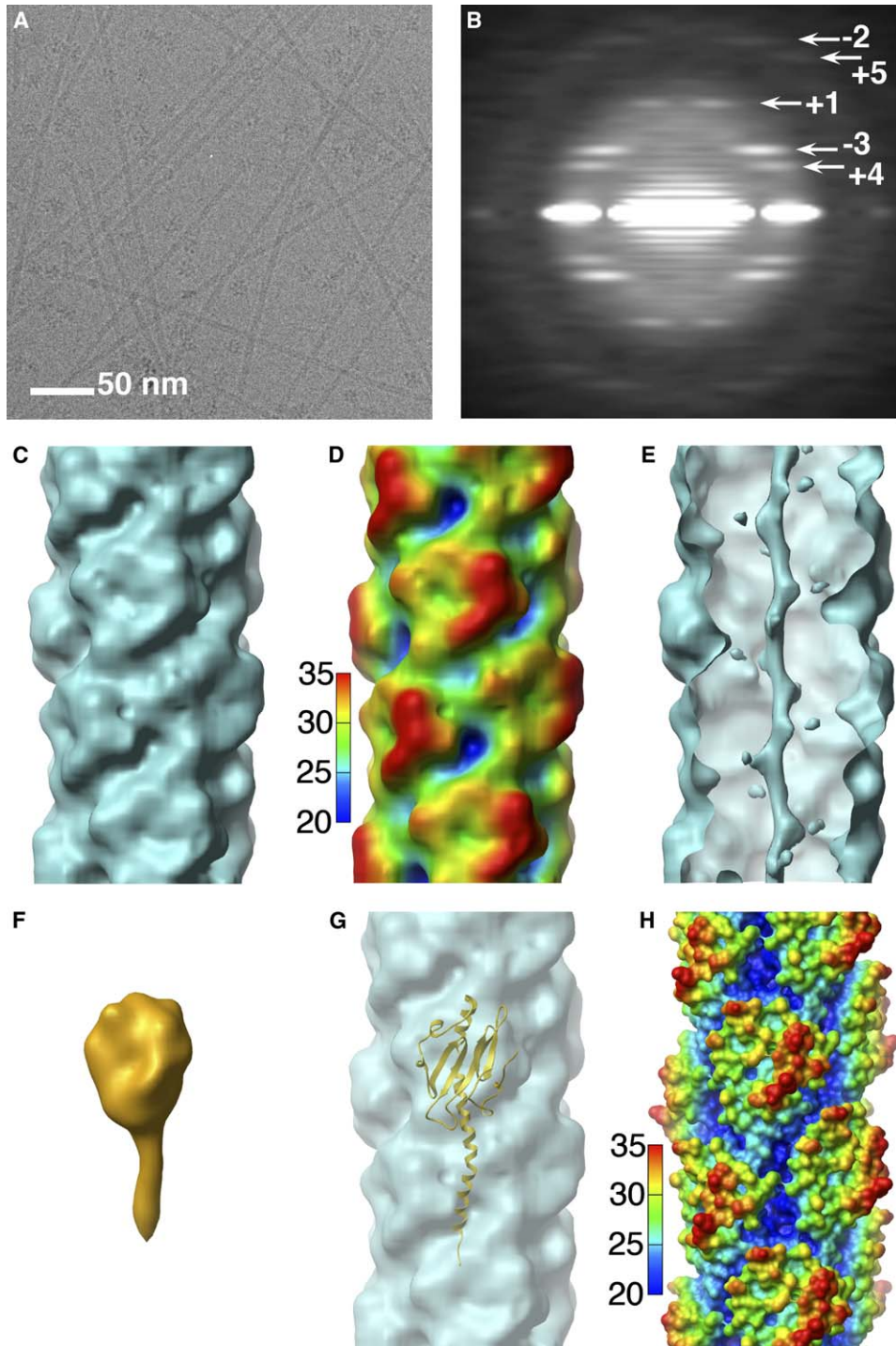


Figure 3. Cryo-EM and 3D Reconstruction of the GC Pilus at 12.5 Å Resolution

(A) GC-T4P in vitreous ice over a carbon hole show smooth surfaces.

(B) Averaged diffraction pattern (power spectra) generated from 24,272 overlapping GC-T4P segments extracted from four micrographs (1.9–2.2 μm defocus). Each segment was 200 pixels long, with a sampling of 2.54 Å/pixel. Layer lines are marked with the principal Bessel orders: $n = +4$, is at 1/87 Å in Fourier space; $n = -3$, 1/64 Å; $n = +1$, 1/37 Å; $n = +5$, 1/26 Å; and $n = -2$, 1/24 Å. Bessel order hand (–, left handed; +, right handed) was determined by fitting the crystallographic subunit into the EM density map.

(C) Filament density map for GC-T4P shows surface grooves and ridges.

(D) Reconstruction in radial distance coloring (based on distance in Å from the fiber axis) highlights filament surface topography.

(E) Filament cutaway shows the tightly packed hydrophobic core with narrow central channel.

(F) GC pilin subunit electron density filtered to 12.5 Å resolution.

(G) Pilin subunit match to cryo-EM density map.

(H) Radial distance coloring of the resultant GC-T4P structure showing the pronounced grooves (blue) between the globular head domains of neighboring subunits. The reconstruction contour level matches the filament model molecular surface. All views match (C).

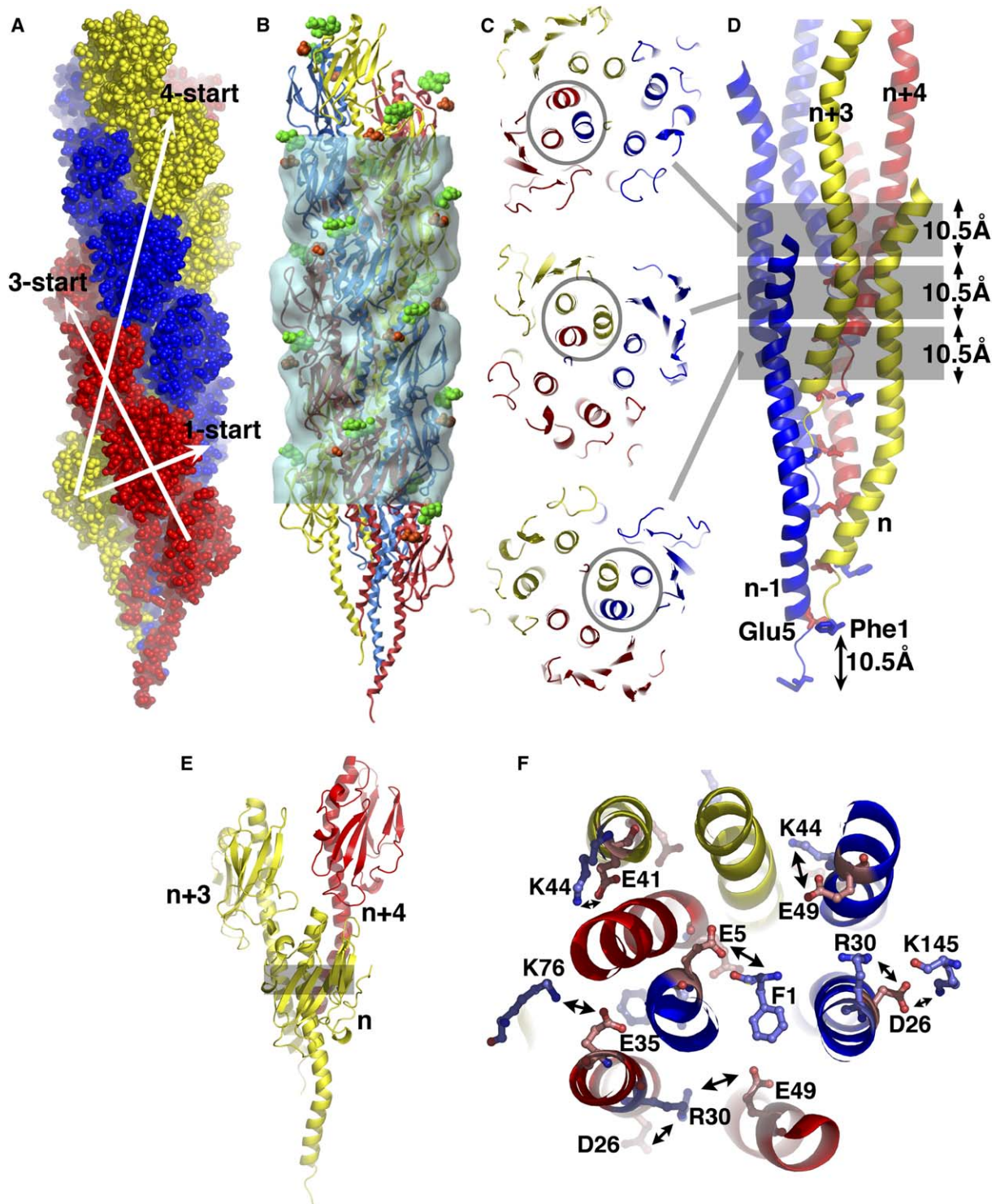


Figure 4. High-Resolution Model of the GC-T4P Filament

(A) Subunits traced along a right-handed 1-start helix, along three strands of a left-handed 3-start helix (colored red, blue, and yellow), and along four strands of a right-handed 4-start helix.

(B) Pilin subunits of GC-T4P within the isosurface of the cryo-EM density map reveal the protruding, surface-exposed disaccharide Gal-DADDGlc (green spheres) and phosphoethanolamine (orange spheres).

(C) Pilin subunit packing of alternating 3-helix bundles that wind up the filament axis and exchange partners every 10.5 Å, matching the subunit axial rise for the 1-start helix. Three consecutive 10.5 Å slabs of the filament illustrate the alternating nature of the 3-helix bundles (circled).

(D) N-terminal α helices (side view) showing the pairing every 10.5 Å of negatively charged Glu5 of one subunit (n-1 in this case) and the positively charged N-terminal Phe1 of the next subunit up (n) in the 1-start helix.

(E) Filament side view showing a trimer of subunits for one 3-helix bundle (shaded area). Subunits are numbered along the 1-start helix.

(F) α -helical core cross-section (20 Å thickness) shows complementarity between charged side chains in the otherwise hydrophobic core.

interact along the strands of the left-handed 3-start helix, and the loops of the β sheet interact axially along the right-handed 4-start helices (Figures 4A and 4B).

The pilin subunits pack remarkably well into the cryo-EM density map (Figure 4B). Only the disaccharide, phosphoethanolamine, and a few long side chains extend beyond the map, as expected for fine protrusions at this resolution. The filament outer diameter is ~ 60 Å. The narrow central channel (Figure 3E) winds along the filament axis with a variable diameter of ~ 6 – 11 Å between atom centers. This hydrophobic channel is unlikely to be solvent filled but may provide a compressible space to account for the extraordinary pilus flexibility seen by EM (Figure 1). The pronounced groove separating the strands of the 3-start helix likely also enhances filament flexibility and moreover appears suitable to mediate key pilus functions by providing receptor-like binding site channels along the filament (see below).

The interactions among the long hydrophobic N-terminal α helices in the GC-T4P core represent $\sim 75\%$ of the 4000 Å² buried surface area for each pilin subunit (calculated with a 1.6 Å probe radius). These $\alpha 1$ helices have a distinctive S-shaped curve (Figures 4B–4F) that results from two kinks, at Pro22 and Gly42, which are conserved among the type IVa pilins (Craig et al., 2004). Overall, each $\alpha 1$ helix lies at a slight angle to the filament axis, with its N terminus near the center and its C terminus at a larger radius. Because the pilin subunits are arranged helically, their α helices are staggered along the filament axis, with neighboring subunits along the right-handed 1-start helix (subunit n , subunit $n+1$, etc.) separated by a rise of 10.5 Å (Figure 4D). Pilin α helices form three-helix bundles that exchange partners every 10.5 Å along the filament axis and wind their way up the filament, anchoring the globular pilin heads (Figures 4C–4E). Each three-helix bundle is formed by α helices from two neighboring subunits in the 3-start helix (subunit n , residues 24–39, and subunit $n+3$, residues 4–19) together with one of the 1-start helix neighbors (subunit $n+4$, residues 1–13).

Along its length, each $\alpha 1$ participates in three distinct three-helix bundles, which are related by the helical symmetry of the filament. Starting from the N terminus, residues 1–13 participate in the first three-helix bundle, overlapping residues 4–19 participate in the second, and residues 24–39 join the third bundle (Figures 4C and 4D). These interaction segments have several β -branched hydrophobic side chains in the α -helical a and d positions, which favor parallel three-helix bundles (Harbury et al., 1993). The N-terminal α -helical interactions that interlock subunits help explain the surprising mechanical strength observed for these extremely thin filaments (Maier et al., 2002) and furthermore place pili within the extensive framework of information on helical coil interactions as mediators of specific protein assemblies.

The protruding half of $\alpha 1$, $\alpha 1$ -N, is almost entirely hydrophobic with only one polar residue, Glu5, in the first 24 amino acids (Figure 2D). The C terminus of $\alpha 1$ -C has both polar and nonpolar residues, including four negatively charged residues, Asp26, Glu35, Glu41, and Glu49, and three positively charged ones, the N-terminal Phe1, Arg30, and Lys44. Each charge is either neutralized by an intrasubunit salt bridge or is close enough to a complementary charge on a neighboring $\alpha 1$ to be

neutralized by an intersubunit salt bridge (Figure 4F). Interestingly, Glu5, which is strictly conserved among the T4P, lies at the same level along the filament axis as the positively charged N terminus of Phe1 of the next subunit up ($n+1$) in the 1-start helix (Figures 4D and 4F). The negatively charged Glu5 O ϵ 2 and positively charged Phe1 N point toward the filament center and are close enough to form a salt bridge. In both the GC pilin crystal structure and the full-length crystal structure of PAK pilin (Craig et al., 2003), the terminal nitrogen forms a salt bridge with Glu5-O ϵ 1 of the same subunit, underscoring the necessity for charge neutralization of the N terminus within a hydrophobic environment. Thus, the N-terminal α helices interact via both hydrophobic and electrostatic interactions, with the overall neutrality of the filament core maintained by both intra- and intersubunit electrostatic interactions that set the register of the subunits along the filament axis.

GC-T4P as a Prototype for T4P

The high-resolution GC-T4P structure determined by combined cryo-EM reconstruction and X-ray crystallography allows the precise placement of subunits within the experimental cryo-EM density (Figures 3 and 4). Based upon these results and analyses, we propose that this GC-T4P structure is a prototype for T4P, providing unified insights to address the paradox of conserved architecture and diverse function. The sequence-conserved N terminus provides the major assembly interface in the filament via twisted three-helix bundle interactions (Figures 4C–4E). These α -helical interactions explain the mechanical strength, whereas gaps between the head domains and within the filament core (Figures 3D and 3E) provide space for pilus flexibility. The helical core structure anchors the globular pilin heads, which also are connected along the 3-start helical strands by interactions between the $\alpha\beta$ loop and D region (Figures 4B and 5). Besides providing contacts between the heads, the structurally variable $\alpha\beta$ loop and D region define the pilus surface chemistry and are implicated in key pilus functions, including receptor binding (Doig et al., 1990), microcolony formation (Kirm et al., 2000), and antigenic variation (Seifert and So, 1984). The dominant role of the N-terminal helix and its helical bundle packing in pilus assembly explain the ability of pilus-associated proteins that act in bacterial virulence, such as *N. meningitidis* PilX, to become integrated into assembled fibers via conservation of the N-terminal helix (Hélaine et al., 2005). In fact, the experimentally defined GC-T4P structure appears suitable as a prototype for the archaeal flagella and for pseudopili formed by the type II secretion pseudopilins based on their N-terminal sequence homology with the type IV pilins as well as common filament features and subunit processing (Peabody et al., 2003).

Antigenicity and Immune Escape

Antibody binding to T4P can block bacterial adhesion (Rothbard et al., 1985), and immunization with pili is protective in some cases (Egerton et al., 1987; Lepper et al., 1995; Taylor et al., 2004), yet antigenic variation of *Neisseria* T4P has limited their efficacy as vaccine candidates (Boslego et al., 1991). The high-resolution structure of GC-T4P explains the observed antipeptide antibody interactions with assembled pili (Forest et al.,

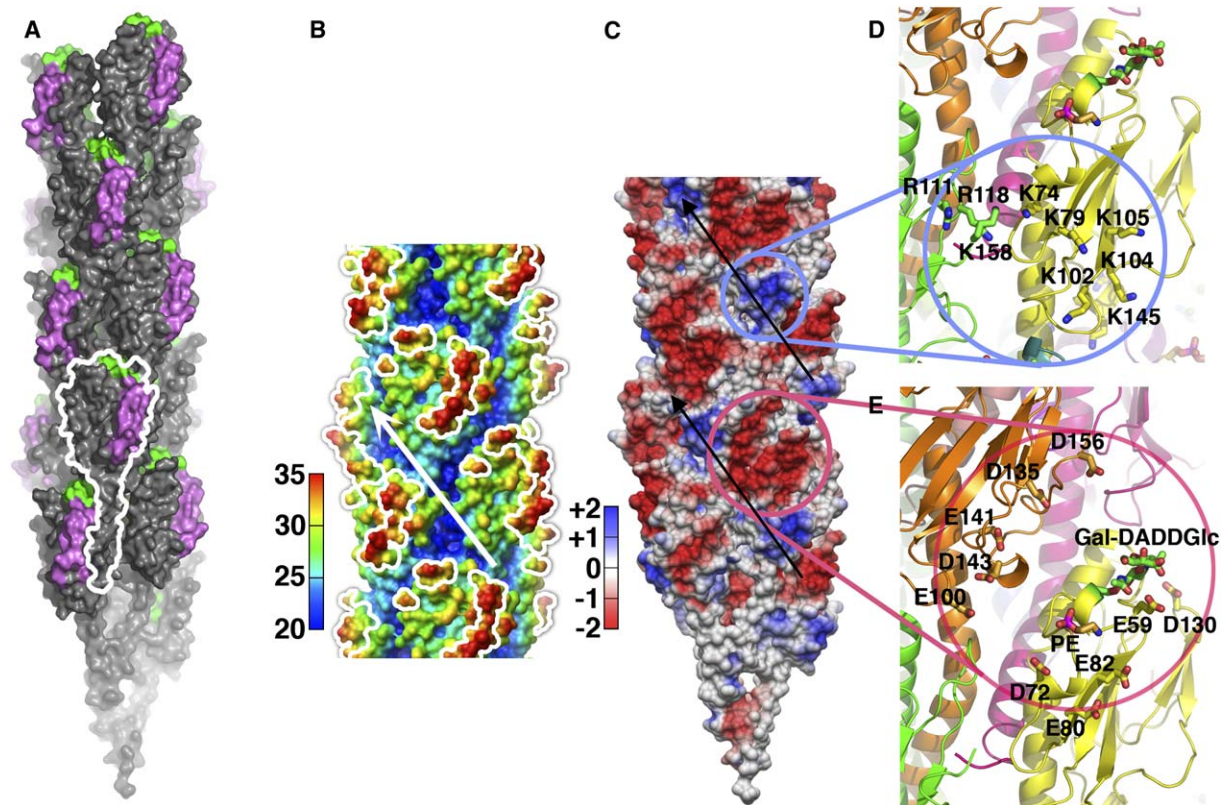


Figure 5. GC-T4P Surface Features and Implications for Immune Evasion, Autoagglutination, and DNA Binding

(A) Epitopes for antibodies that bind only the GC-T4P tips (peptide 37-56, green) are buried along the filament length by intersubunit interactions and only fully accessible at one end of the filament, whereas epitopes for side binding antibodies (peptide 122-139, pink) are fully exposed (Forest et al., 1996).

(B) Radial distance map (Å) reveals the posttranslational modifications and the hypervariable region (outlined in white) as the most protruding filament features and the deep groove that follows the left-handed 3-start helix (arrow).

(C) Filament electrostatic surface (calculated with UHBD [Madura et al., 1995]) shows the alternating negative (red) and positive (blue) charge regions, with positive patches providing possible extended DNA binding sites within grooves (black arrows) between the 3-start helices.

(D) Positive patch formed by basic residues in the $\alpha\beta$ loop and C terminus of one subunit (yellow) and residues flanking the D region of a neighboring subunit (green) in the right-handed 1-start helix.

(E) Negative patch formed by acidic residues in the $\alpha\beta$ loop of one subunit (yellow) and the D region of a neighboring subunit (orange) in the left-handed 3-start helix with green disaccharide (Gal-DADDGlc) and orange phosphoethanolamine (PE) carbons.

1996). For example, antibodies to peptide 37-56 (i.e., residues 37-56) bound the tips of the GC-T4P, but not the sides. Our GC-T4P structure shows that this epitope is obscured by subunit-subunit interactions along the filament length but is exposed at the filament tip (green patches, Figure 5A). Epitope 37-56 is of particular interest as antisera from human volunteers immunized with whole pili or infected with *N. gonorrhoeae* bind to residues 47-56 within this epitope (Boslego et al., 1991), and this region is implicated in gonococcal attachment to endocervical cells (Rothbard et al., 1985). In contrast, epitopes bound by antibodies along the filament length are fully exposed all along our GC-T4P structure (e.g., peptide 122-139, pink patches, Figure 5A).

In the GC-T4P structure, the pilin subunit regions that are most accessible to antibodies are also the most variable: the $\alpha\beta$ loop with its variable amino acids and post-translational modifications, and the D region hypervariable loop. These regions protrude from the filament surface and obscure the less-variable β sheet (Figures 2A and 5B). To design effective T4P-based vaccines, it will be necessary to redirect the immune response to

the less-accessible conserved epitopes on GC-T4P, which are more likely to elicit broadly neutralizing antibodies for *Neisseriae*, or toward functionally important but low abundance pilus-associated proteins that assemble via the N-terminal helix interactions. As the extreme antigenic variation seen for GC-T4P does not occur in other Gram-negative bacterial pathogens, T4P remain attractive vaccine targets.

Natural Transformation

The well-characterized role of *Neisseria* T4P in binding and uptake of double-stranded DNA is shared by other bacterial T4P (Hamilton and Dillard, 2006). The high-resolution T4P structure reveals charged grooves suitable for this process. The most striking groove follows the left-handed 3-start helix and penetrates the filament surface by as much as 15 Å at its deepest point (Figure 5B). This groove is formed at the interface between subunits in the 1-start helix and is lined with patches of positively charged side chains, which are either conserved or semiconserved in the GC pilin sequence (Figures 5C and 5D). These basic residues are contributed by the

D region of one subunit and the $\alpha\beta$ loop of the next along the 1-start helix. The positively charged groove is wide enough to bind the negatively charged backbone of double-stranded DNA, providing a mechanism for the role of GC-T4P in natural transformation (Aas et al., 2002). Exogenous DNA strands could wrap around the GC-T4P surface via nonspecific electrostatic interactions for transport into the periplasm via pilus retraction. An extended positively charged surface patch was also proposed for *Pseudomonas* type IV pili, which binds DNA without sequence specificity (van Schaik et al., 2005). Besides the positively charged residues, other residues lining the main GC-T4P groove are conserved among GC pilins. Thus, this functional groove is an attractive target for binding of specific antibacterial agents for transport into the cell.

Cell Adhesion and Microcolony Formation

T4P play key roles in both host cell attachment and microcolony formation (via pilus-pilus interactions) (Craig et al., 2004). Although GC-T4P utilize a tip-associated adhesion protein, PilC, for binding to host cell receptors, the GC pilin subunits also act directly in adhesion (Jonsson et al., 1994; Nassif et al., 1993). Antibodies or peptides that specifically bind T4P can block bacterial adhesion to cultured cells (Rothbard et al., 1985; Wu et al., 2005). Furthermore, pilus-based adhesion is intimately linked with bacterial motility, as the cells must adhere to surfaces to be pulled along by T4P retraction. In the GC-T4P structure, the positively charged surface patches described above alternate with negatively charged patches and provide possible complementary extended sites for pilus interactions in microcolony formation and adhesion to cell receptor carbohydrates. The negative patches are formed by acidic residues in the globular domain interfaces of the left-handed 3-start helices, between the $\alpha\beta$ loop and D region of adjacent subunits (Figures 5C and 5E). Charged residues in the D region are directly involved in TCP-mediated microcolony formation in *V. cholerae* (Kirn et al., 2000). Both the phosphoethanolamine and the disaccharide lie on the negative patches, and thus, varying these modifications would likely modulate the adhesion properties. This charge distribution also explains our in vitro observation that T4P are soluble at basic pH, where the pili would have an overall negative charge, but form insoluble aggregates at neutral pH, where alternating patches of charge complementarity would promote pilus-pilus interactions. Furthermore, the deep grooves along the filament resemble extended substrate binding sites for DNA, carbohydrate, and protein domains (Figures 5B–5E). Thus, the charged, corrugated T4P surface revealed in our GC-T4P structure suggests a means by which pili accomplish diverse binding events, including both adherence to host cell surfaces and to other bacteria.

T4P Assembly-Disassembly and Motility

T4P switch between assembly and disassembly from a reservoir of inner membrane pilin subunits to accomplish twitching motility, which is critical for pathogen movement on host cell surfaces (Merz et al., 2000; Wolfgang et al., 1998) and can include T4P pole-to-pole oscillations to direct motion (Mignot et al., 2005). GC-T4P disassembly (retraction) is required for efficient

DNA uptake in *N. gonorrhoeae* (Aas et al., 2002) and for dispersal from microcolonies and dissemination throughout the small intestine in enteropathogenic *E. coli* (Anantha et al., 2000; Bieber et al., 1998). Recently, GC pilus retraction was implicated in pilus-induced Ca^{2+} mobilization in host epithelial cells, which may function in gonococcal invasion and intracellular survival (Ayala et al., 2005). GC-T4P retraction could bring the bacterial and host cell membranes into direct contact, allowing bacterial porin to insert into the host cell membrane and trigger Ca^{2+} influx. In addition, retraction of bound pili may exert substantial stress forces on the host cell membrane that could signal downstream effects. The mechanism by which bacteria rapidly assemble and retract their T4P thus underlies many T4P-based functions in pathogenicity.

We therefore propose here a generalized mechanism for T4P assembly-disassembly based on our GC-T4P structure and commonalities among the T4P, including a conserved pilin subunit structural core, a left-handed 3-start helical filament architecture, and conserved components of the pilus biogenesis apparatus across different species (Craig et al., 2004). In our model, pilin subunits in the inner membrane are added to each of the 3-start helical strands at three active sites around the filament circumference (a single active site is shown in Figure 6). The addition of each pilin subunit would stabilize the hydrophobic α helices of two existing subunits in the growing filament, completing a subunit trimer and forming a new three-helix bundle. This 3-start assembly mechanism would obviate the need for substantial conformational changes of the N-terminal helix or rotations of either the growing filament or the assembly apparatus upon addition of each new pilin subunit. We propose the following sequence of events: (1) subunit n adds to the growing filament by diffusion and electrostatic attraction, (2) the pilus assembly ATPase on the cytosolic face of the inner membrane hydrolyzes ATP (Crowther et al., 2005), (3) ATP hydrolysis induces a piston-like motion in an associated membrane binding partner (MBP), (4) the pilus filament is translated 10.5 Å out of the membrane, and (5) ATP replaces bound ADP, allowing the MBP to relax to its original position.

This 3-start assembly model is consistent with the observation that BfpD, the hexameric ATPase required for bundle-forming pilus assembly in enteropathogenic *E. coli*, binds only three BfpE (MBP) molecules at one time. Also, the BfpE site that interacts with BfpD shifts depending on whether ATP or ADP is bound to BfpD (Crowther et al., 2005). The presence of the positively charged N-terminal Phe1 on the terminal pilin subunit in the growing filament would provide a polar interaction for the conserved Glu5 of the incoming subunit in an otherwise hydrophobic environment. Furthermore, the distance that the pilus filament must be extruded out of the membrane need only span the rise of a single subunit in the 1-start helix (10.5 Å or ~ 2 α -helical turns). Addition of three subunits, one to each strand of the 3-start helix, would result in a new 31.5 Å gap created at the first strand, which could then accommodate a new subunit. The joining of a subunit, n , to the growing filament would complete a new three-helix bundle started by subunits $n+3$ and $n+4$, thus shielding hydrophobic regions in $\alpha 1$ from the periplasm as the filament is extruded from the

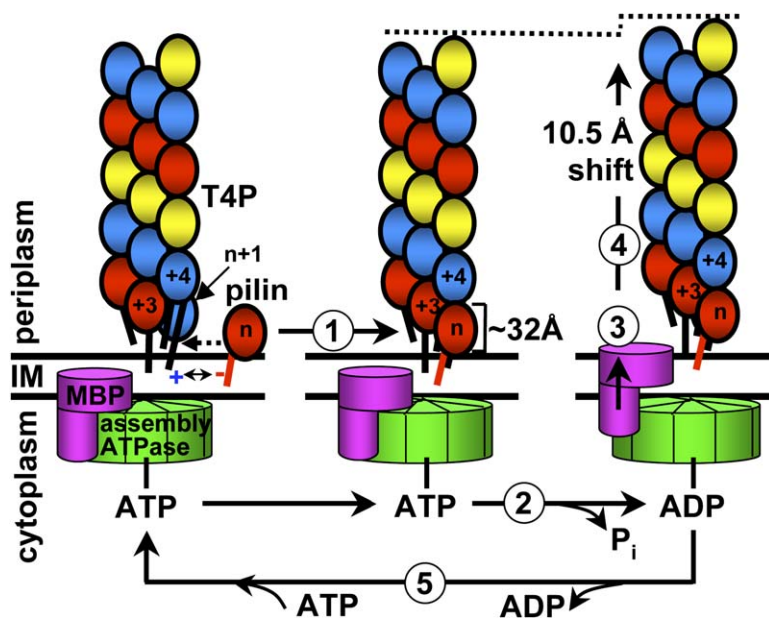


Figure 6. Proposed T4P Assembly Mechanism at the Inner Membrane

Pilin subunits are solubilized in the inner membrane (IM) by complementarity of their hydrophobic N-terminal α helix with the lipid bilayer and positively charged globular domain bottoms with the negatively charged phospholipid head groups. Subunits add to the growing filament, in part by charge complementarity between Glu5 of the incoming subunit (n) and Phe1 of the existing n+1 subunit, numbered along the 1-start helix. Addition of subunit n to the growing filament completes the three-helix bundle and subunit trimer formed by n, n+3, and n+4. (1) Subunit n binds to the growing filament, (2) one molecule of ATP, which is bound to the hexameric assembly ATPase on the cytoplasmic side of the IM, is hydrolyzed, (3) ATP hydrolysis induces a piston-like motion in the ATPase membrane binding partner (MBP), (4) which drives the growing filament outward toward the periplasm a distance of 10.5 Å, and (5) ADP is exchanged for ATP, allowing the assembly apparatus to relax to its resting position. This mechanism may occur consecutively at three active sites on the ATPase, one for each strand of the 3-start helix (shown here in red, blue, and yellow). Three consecutive ATP hydrolysis events would push the filament out 10.5 Å, resulting in a 31.5 Å gap at the first site to accommodate a new subunit.

inner membrane. This mechanistic model is generalizable to all T4P, with the extrusion distance depending on the pilin globular domain size. It furthermore provides a basis to incorporate pilus-associated proteins with variable globular domains and functions, such as *N. meningitidis* PilX, which possess the N-terminal helix (H elaine et al., 2005). The mechanism would be reversed for disassembly with a retraction ATPase displacing the assembly ATPase to power dissociation of the subunits via reversal of the MBP piston (Merz et al., 2000).

Importantly, our proposed 3-start mechanism would allow rapid T4P assembly and disassembly, as required for its roles in twitching motility, DNA uptake, microcolony dispersion, and signaling. For many functions, pilus retraction is intimately linked to adhesion and thus any retraction model must consider release of pili from bound substrates, including DNA, other pili in microcolonies, and host cell receptors. Adhesion is likely to occur through multiple weak interactions via T4P surface channels, resulting in a strong pilus-substrate bond due to avidity. ATP-driven pilus retraction would disrupt these weak electrostatic interactions one by one with minimal energy cost. This would occur at the outer membrane for pilus-pilus and pilus-host cell interactions and at the inner membrane for DNA uptake. Our 3-start assembly-disassembly model thus provides a molecular framework to test and understand mechanisms for the complex and fundamental processes of T4P binding and movement in bacterial pathogenesis.

Overall Implications

Previous T4P filament models failed to explain (a) the paradox of a conserved, mechanically sound architecture coupled with flexibility, multifunctionality, and extreme sequence variation, (b) the incorporation of

pilus-associated proteins, or (c) the combination of binding and movement provided by T4P, which is a defining characteristic of bacterial pathogens (Mattick, 2002). The integrated crystallographic and cryo-EM results presented here help address these issues by defining the detailed assembled molecular structure of a prototypic T4P. Surface protrusions allow antigenic variation and reversible pilus-pilus interactions, whereas grooves provide protected DNA, protein, and carbohydrate binding sites. Overall, this structure reveals how a conserved molecular architecture for T4P provides the corrugated surface, strength, flexibility, and efficient assembly-disassembly capabilities needed for motility, natural transformation, and other diverse functions. The structural detail also provides a foundation for understanding such surprising activities as electron transfer, as recently observed for T4P from the Geobacter species (Reguera et al., 2005). Surface channels may provide receptor-like binding sites for chains of electron transfer proteins or cofactors. Thus, the T4P structure provides an informed basis for understanding and genetically modifying pilin to generate predetermined and different functionalities without disrupting assembly interactions. Such engineering has relevance for designing T4P-based vaccines as well as biologically produced nanowires and other filament assemblies. The identified T4P grooves also provide targets for the design of small molecule inhibitors as pathogen blockers, consistent with recent experimental results showing that a T4P binding peptide specifically inhibits *S. typhi* adhesion to, and invasion of, human monocytes (Wu et al., 2005). These results thus suggest a unified T4P architecture and assembly mechanism whereby ATP-driven pilus translation from the inner membrane allows spiraling three-helix bundles to form strong but flexible filament

cores, anchoring variable globular heads for their distinct cellular functions. This assembly model permits incorporation of pilus-associated proteins and may also describe assembly and architecture of the structurally related archaeal flagella and type II secretion system filaments.

Experimental Procedures

Purification of Native GC Pilus Filaments and Pilin Subunits

The GC-T4P filaments and GC pilin subunits used in the structural analyses were purified from *N. gonorrhoeae* strain C30 cells as described in the [Supplemental Data](#).

Crystallization, Crystallographic Data Collection, Structure Determination, and Refinement of GC Pilin

Data collection and refinement statistics and methods are described in the [Supplemental Data](#).

Cryo-EM and Iterative Helical Real Space Reconstruction

The 3D reconstruction of the GC-T4P filament was determined with cryo-EM images of pilus filaments using the IHRSR algorithm (Egelman, 2000) (see [Supplemental Data](#)).

Computational Docking of GC Pilin Structure into the Cryo-EM Reconstruction

The methodologies for docking and generation of a helical filament are described in the [Supplemental Data](#).

Figure Preparation

See the [Supplemental Data](#).

Supplemental Data

Supplemental Data include Supplemental Experimental Procedures and Supplemental References and can be found with this article online at <http://www.molecule.org/cgi/content/full/23/5/651/DC1>.

Acknowledgments

We thank Lucas Liu for technical assistance; Michael Donnenberg, Brian Adair, Atsushi Yamagata, Katrina Forest, Michael Koomey, David Vocado, and Andrew Bennett for discussions; Scott Williams, Elizabeth Getzoff, and Erika Plettner for comments on the manuscript; and the staff at Beamline 7-1 at Stanford Synchrotron Radiation Laboratories for diffraction facilities. This work was supported by National Institutes of Health grants AI22160 (J.A.T. and L.C.), EB001567 (E.H.E.), GM066087 (M.Y.), and GM076503 (N.V.) and a fellowship from The Canadian Institutes of Health Research (L.C.).

Received: April 5, 2006

Revised: May 16, 2006

Accepted: July 10, 2006

Published: August 31, 2006

References

Aas, F.E., Wolfgang, M., Frye, S., Dunham, S., Lovold, C., and Koomey, M. (2002). Competence for natural transformation in *Neisseria gonorrhoeae*: components of DNA binding and uptake linked to type IV pilus expression. *Mol. Microbiol.* **46**, 749–760.

Anantha, R.P., Stone, K.D., and Donnenberg, M.S. (2000). Effects of *bfp* mutations on biogenesis of functional enteropathogenic *Escherichia coli* type IV pili. *J. Bacteriol.* **182**, 2498–2506.

Audette, G.F., Irvin, R.T., and Hazes, B. (2004). Crystallographic analysis of the *Pseudomonas aeruginosa* strain K122-4 monomeric pilin reveals a conserved receptor-binding architecture. *Biochemistry* **43**, 11427–11435.

Ayala, P., Wilbur, J.S., Wetzler, L.M., Tainer, J.A., Snyder, A., and So, M. (2005). The pilus and porin of *Neisseria gonorrhoeae* cooperatively induce Ca(2+) transients in infected epithelial cells. *Cell. Microbiol.* **7**, 1736–1748.

Bieber, D., Ramer, S.W., Wu, C.Y., Murray, W.J., Tobe, T., Fernandez, R., and Schoolnik, G.K. (1998). Type IV pili, transient bacterial aggregates, and virulence of enteropathogenic *Escherichia coli*. *Science* **280**, 2114–2118.

Boslego, J.W., Tramont, E.C., Chung, R.C., McChesney, D.G., Ciak, J., Sadoff, J.C., Piziak, M.V., Brown, J.D., Brinton, C.C., Jr., Wood, S.W., et al. (1991). Efficacy trial of a parenteral gonococcal pilus vaccine in men. *Vaccine* **9**, 154–162.

Craig, L., Taylor, R.K., Pique, M.E., Adair, B.D., Arvai, A.S., Singh, M., Lloyd, S.J., Shin, D.S., Getzoff, E.D., Yeager, M., et al. (2003). Type IV pilin structure and assembly: X-ray and EM analyses of *Vibrio cholerae* toxin-coregulated pilus and *Pseudomonas aeruginosa* PAK pilin. *Mol. Cell* **11**, 1139–1150.

Craig, L., Pique, M.E., and Tainer, J.A. (2004). Type IV pilus structure and bacterial pathogenicity. *Nat. Rev. Microbiol.* **2**, 363–378.

Criss, A.K., Kline, K.A., and Seifert, H.S. (2005). The frequency and rate of pilin antigenic variation in *Neisseria gonorrhoeae*. *Mol. Microbiol.* **58**, 510–519.

Crowther, L.J., Yamagata, Y., Craig, L., Tainer, J.A., and Donnenberg, M.S. (2005). The ATPase activity of BfpD is greatly enhanced by zinc and allosteric interactions with other Bfp proteins. *J. Biol. Chem.* **280**, 24839–24848.

Doig, P., Sastry, P.A., Hodges, R.S., Lee, K.K., Paranchych, W., and Irvin, R.T. (1990). Inhibition of pilus-mediated adhesion of *Pseudomonas aeruginosa* to human buccal epithelial cells by monoclonal antibodies directed against pili. *Infect. Immun.* **58**, 124–130.

Egelman, E.H. (2000). A robust algorithm for the reconstruction of helical filaments using single-particle methods. *Ultramicroscopy* **85**, 225–234.

Egerton, J.R., Cox, P.T., Anderson, B.J., Kristo, C., Norman, M., and Mattick, J.S. (1987). Protection of sheep against footrot with a recombinant DNA-based fimbrial vaccine. *Vet. Microbiol.* **14**, 393–409.

Forest, K.T., Bernstein, S.L., Getzoff, E.D., So, M., Tribbick, G., Geyesen, H.M., Deal, C.D., and Tainer, J. (1996). Assembly and antigenicity of the *Neisseria gonorrhoeae* pilus mapped with antibodies. *Infect. Immun.* **64**, 644–652.

Forest, K.T., Dunham, S.A., Koomey, M., and Tainer, J.A. (1999). Crystallographic structure reveals phosphorylated pilin from *Neisseria*: phosphoserine sites modify type IV pilus surface chemistry and fibre morphology. *Mol. Microbiol.* **31**, 743–752.

Gil, H., Benach, J.L., and Thanassi, D.G. (2004). Presence of pili on the surface of *Francisella tularensis*. *Infect. Immun.* **72**, 3042–3047.

Giltner, C.L., van Schaik, E.J., Audette, G.F., Kao, D., Hodges, R.S., Hassett, D.J., and Irvin, R.T. (2006). The *Pseudomonas aeruginosa* type IV pilin receptor binding domain functions as an adhesin for both biotic and abiotic surfaces. *Mol. Microbiol.* **59**, 1083–1096.

Giron, J.A., Ho, A.S., and Schoolnik, G.K. (1991). An inducible bundle-forming pilus of enteropathogenic *Escherichia coli*. *Science* **254**, 710–713.

Haas, R., and Meyer, T.F. (1986). The repertoire of silent pilus genes in *Neisseria gonorrhoeae*: evidence for gene conversion. *Cell* **44**, 107–115.

Hamilton, H.L., and Dillard, J.P. (2006). Natural transformation of *Neisseria gonorrhoeae*: from DNA donation to homologous recombination. *Mol. Microbiol.* **59**, 376–385.

Harauz, G., and van Heel, M. (1986). Exact filters for general geometry three dimensional reconstruction. *Optik* **73**, 146–156.

Harbury, P.B., Zhang, T., Kim, P.S., and Alber, T. (1993). A switch between two-, three-, and four-stranded coiled coils in GCN4 leucine zipper mutants. *Science* **262**, 1401–1407.

Hegge, F.T., Hitchen, P.G., Aas, F.E., Kristiansen, H., Lovold, C., Egge-Jacobsen, W., Panico, M., Leong, W.Y., Bull, V., Virji, M., et al. (2004). Unique modifications with phosphocholine and phosphoethanolamine define alternate antigenic forms of *Neisseria gonorrhoeae* type IV pili. *Proc. Natl. Acad. Sci. USA* **101**, 10798–10803.

Hélaine, S., Carbonnelle, E., Prouvensier, L., Beretti, J.L., Nassif, X., and Pelicci, V. (2005). PilX, a pilus-associated protein essential for bacterial aggregation, is a key to pilus-facilitated attachment of *Neisseria meningitidis* to human cells. *Mol. Microbiol.* **55**, 65–77.

- Hsieh, J.C., Tham, D.M., Feng, W., Huang, F., Embaie, S., Liu, K., Dean, D., Hertle, R., Fitzgerald, D.J., and Msrny, R.J. (2005). Intranasal immunization strategy to impede pilin-mediated binding of *Pseudomonas aeruginosa* to airway epithelial cells. *Infect. Immun.* **73**, 7705–7717.
- Jonsson, A.B., Ilver, D., Falk, P., Pepose, J., and Normark, S. (1994). Sequence changes in the pilus subunit lead to tropism variation of *Neisseria gonorrhoeae* to human tissue. *Mol. Microbiol.* **13**, 403–416.
- Keizer, D.W., Slupsky, C.M., Kalisiak, M., Campbell, A.P., Crump, M.P., Sastry, P.A., Hazes, B., Irvin, R.T., and Sykes, B.D. (2001). Structure of a pilin monomer from *Pseudomonas aeruginosa*: implications for the assembly of pili. *J. Biol. Chem.* **276**, 24186–24193.
- Kirn, T.J., Lafferty, M.J., Sandoe, C.M., and Taylor, R.K. (2000). Delineation of pilin domains required for bacterial association into microcolonies and intestinal colonization by *Vibrio cholerae*. *Mol. Microbiol.* **35**, 896–910.
- Lepper, A.W., Atwell, J.L., Lehrbach, P.R., Schwartzkoff, C.L., Eger-ton, J.R., and Tennent, J.M. (1995). The protective efficacy of cloned *Moraxella bovis* pili in monovalent and multivalent vaccine formulations against experimentally induced infectious bovine keratoconjunctivitis (IBK). *Vet. Microbiol.* **45**, 129–138.
- Madura, J.D., Briggs, J.M., Wade, R.C., Davis, M.E., Luty, B.A., Ilin, A., Antosiewicz, J., Gilson, M.K., Bagheri, B., Scott, L.R., and McCammon, J.A. (1995). Electrostatics and diffusion of molecules in solution: simulations with the University of Houston Brownian Dynamics Program. *Comp. Phys. Commun.* **91**, 57–95.
- Maier, B., Potter, L., So, M., Seifert, H.S., and Sheetz, M.P. (2002). Single pilus motor forces exceed 100 pN. *Proc. Natl. Acad. Sci. USA* **99**, 16012–16017.
- Marceau, M., and Nassif, X. (1999). Role of glycosylation at Ser63 in production of soluble pilin in pathogenic *Neisseria*. *J. Bacteriol.* **181**, 656–661.
- Marceau, M., Forest, K., Beretti, J.L., Tainer, J., and Nassif, X. (1998). Consequences of the loss of O-linked glycosylation of meningococcal type IV pilin on piliation and pilus-mediated adhesion. *Mol. Microbiol.* **27**, 705–715.
- Mattick, J.S. (2002). Type IV pili and twitching motility. *Annu. Rev. Microbiol.* **56**, 289–314.
- Merz, A.J., and So, M. (2000). Interactions of pathogenic *Neisseriae* with epithelial cell membranes. *Annu. Rev. Cell Dev. Biol.* **16**, 423–457.
- Merz, A.J., So, M., and Sheetz, M.P. (2000). Pilus retraction powers bacterial twitching motility. *Nature* **407**, 98–102.
- Mignot, T., Merlie, J.P., Jr., and Zusman, D.R. (2005). Regulated pole-to-pole oscillations of a bacterial gliding motility protein. *Science* **310**, 855–857.
- Morand, P.C., Bille, E., Morelle, S., Eugene, E., Beretti, J.L., Wolfgang, M., Meyer, T.F., Koomey, M., and Nassif, X. (2004). Type IV pilus retraction in pathogenic *Neisseria* is regulated by the PilC proteins. *EMBO J.* **23**, 2009–2017.
- Nassif, X., Lowy, J., Stenberg, P., O'Gaora, P., Ganji, A., and So, M. (1993). Antigenic variation of pilin regulates adhesion of *Neisseria meningitidis* to human epithelial cells. *Mol. Microbiol.* **8**, 719–725.
- Parge, H.E., Forest, K.T., Hickey, M.J., Christensen, D.A., Getzoff, E.D., and Tainer, J.A. (1995). Structure of the fibre-forming protein pilin at 2.6 Å resolution. *Nature* **378**, 32–38.
- Peabody, C.R., Chung, Y.J., Yen, M.R., Vidal-Ingigliardi, D., Pugsley, A.P., and Saier, M.H., Jr. (2003). Type II protein secretion and its relationship to bacterial type IV pili and archaeal flagella. *Microbiol.* **149**, 3051–3072.
- Plant, L.J., and Jonsson, A.B. (2006). Type IV pili of *Neisseria gonorrhoeae* influence the activation of human CD4+ T cells. *Infect. Immun.* **74**, 442–448.
- Power, P.M., Roddam, L.F., Rutter, K., Fitzpatrick, S.Z., Srikhanta, Y.N., and Jennings, M.P. (2003). Genetic characterization of pilin glycosylation and phase variation in *Neisseria meningitidis*. *Mol. Microbiol.* **49**, 833–847.
- Reguera, G., McCarthy, K.D., Mehta, T., Nicoll, J.S., Tuominen, M.T., and Lovley, D.R. (2005). Extracellular electron transfer via microbial nanowires. *Nature* **435**, 1098–1101.
- Rothbard, J.B., Fernandez, R., Wang, L., Teng, N.N., and Schoolnik, G.K. (1985). Antibodies to peptides corresponding to a conserved sequence of gonococcal pilins block bacterial adhesion. *Proc. Natl. Acad. Sci. USA* **82**, 915–919.
- Rudel, T., Scheurerpflug, I., and Meyer, T.F. (1995). *Neisseria* PilC protein identified as type-4 pilus tip-located adhesin. *Nature* **373**, 357–359.
- Segal, E., Hagblom, P., Seifert, H.S., and So, M. (1986). Antigenic variation of gonococcal pilus involves assembly of separated silent gene segments. *Proc. Natl. Acad. Sci. USA* **83**, 2177–2181.
- Seifert, H., and So, M. (1984). Genetic mechanisms of bacterial antigenic variation. *Microbiol. Rev.* **52**, 327–336.
- Stimson, E., Virji, M., Makepeace, K., Dell, A., Morris, H.R., Payne, G., Saunders, J.R., Jennings, M.P., Barker, S., Panico, M., et al. (1995). Meningococcal pilin: a glycoprotein substituted with digalactosyl 2,4-diacetamido-2,4,6-trideoxyhexose. *Mol. Microbiol.* **17**, 1201–1214.
- Swanson, J., Bergstrom, S., Robbins, K., Barrera, O., Corwin, D., and Koomey, J.M. (1986). Gene conversion involving the pilin structural gene correlates with pilus+ in equilibrium with pilus– changes in *Neisseria gonorrhoeae*. *Cell* **47**, 267–276.
- Taylor, R.K., Miller, V.L., Furlong, D.B., and Mekalanos, J.J. (1987). Use of *phoA* gene fusions to identify a pilus colonization factor coordinately regulated with cholera toxin. *Proc. Natl. Acad. Sci. USA* **84**, 2833–2837.
- Taylor, R.K., Kirn, T.J., Meeks, M.D., Wade, T.K., and Wade, W.F. (2004). A *Vibrio cholerae* classical TcpA amino acid sequence induces protective antibody that binds an area hypothesized to be important for toxin-coregulated pilus structure. *Infect. Immun.* **72**, 6050–6060.
- Tobiason, D.M., and Seifert, H.S. (2006). The Obligate Human Pathogen, *Neisseria gonorrhoeae*, Is Polyploid. *PLoS Biol.* **4**, e185. 10.1371/journal.pbio.0040185.
- van Schaik, E.J., Giltner, C.L., Audette, G.F., Keizer, D.W., Bautista, D.L., Slupsky, C.M., Sykes, B.D., and Irvin, R.T. (2005). DNA binding: a novel function of *Pseudomonas aeruginosa* type IV pili. *J. Bacteriol.* **187**, 1455–1464.
- Volkman, N., and Hanein, D. (2003). Docking of atomic models into reconstructions from electron microscopy. *Methods Enzymol.* **374**, 204–225.
- Weiser, J.N., Goldberg, J.B., Pan, N., Wilson, L., and Virji, M. (1998). The phosphorylcholine epitope undergoes phase variation on a 43-kilodalton protein in *Pseudomonas aeruginosa* and on pili of *Neisseria meningitidis* and *Neisseria gonorrhoeae*. *Infect. Immun.* **66**, 4263–4267.
- Wolfgang, M., Park, H.S., Hayes, S.F., van Putten, J.P., and Koomey, M. (1998). Suppression of an absolute defect in type IV pilus biogenesis by loss-of-function mutations in *pilT*, a twitching motility gene in *Neisseria gonorrhoeae*. *Proc. Natl. Acad. Sci. USA* **95**, 14973–14978.
- Wu, H.Y., Zhang, X.L., Pan, Q., and Wu, J. (2005). Functional selection of a type IV pili-binding peptide that specifically inhibits *Salmonella Typhi* adhesion to/invasion of human monocytic cells. *Peptides* **26**, 2057–2063.
- Xu, X.F., Tan, Y.W., Lam, L., Hackett, J., Zhang, M., and Mok, Y.K. (2004). NMR structure of a type IVb pilin from *Salmonella typhi* and its assembly into pilus. *J. Biol. Chem.* **279**, 31599–31605.
- Yang, S., Yu, X., Galkin, V.E., and Egelman, E.H. (2003). Issues of resolution and polymorphism in single-particle reconstruction. *J. Struct. Biol.* **144**, 162–171.
- Zhang, X.L., Tsui, I.S., Yip, C.M., Fung, A.W., Wong, D.K., Dai, X., Yang, Y., Hackett, J., and Morris, C. (2000). *Salmonella enterica* serovar typhi uses type IVb pili to enter human intestinal epithelial cells. *Infect. Immun.* **68**, 3067–3073.

Accession Numbers

The structures described in this paper are deposited in the Protein Data Bank under accession numbers 2HI2 (GC pilin) and 2HIL (GC-T4P). The cryo-EM density map for GC-T4P is available in the Electron Microscopy Data Bank (<http://www.ebi.ac.uk/msd>) under accession number EM-1236.